CrossMark

Brazilian Test of Concrete Specimens Subjected to Different Loading Geometries: Review and New Insights

Víctor J. García[1,2],*, Carmen O. Márquez[2,3], Alonso R. Zúñiga-Suárez[1],
Berenice C. Zuñiga-Torres[1], and Luis J. Villalta-Granda[1]

Abstract: The objective of this work was finding out the most advisable testing conditions for an effective and robust characterization of the tensile strength (TS) of concrete disks. The independent variables were the loading geometry, the angle subtended by the contact area, disk diameter and thickness, maximum aggregate size, and the sample compression strength (CS). The *effect* of the independent variables was studied in a three groups of experiments using a factorial design with two levels and four factors. The likeliest location where failure beginning was calculated using the equations that account for the stress–strain field developed within the disk. The theoretical outcome shows that for failure beginning at the geometric center of the sample, it is necessary for the contact angle in the loading setup to be larger than or equal to a threshold value. Nevertheless, the measured indirect tensile strength must be adjusted to get a close estimate of the uniaxial TS of the material. The correction depends on the loading geometry, and we got their mathematical expression and cross-validated them with the reported in the literature. The experimental results show that a loading geometry with a curved contact area, uniform load distribution over the contact area, loads projected parallel to one another within the disk, and a contact angle bigger of 12° is the most advisable and robust setup for implementation of BT on concrete disks. This work provides a description of the BT carries on concrete disks and put forward a characterization technique to study costly samples of cement based material that have been enabled to display new and improved properties with nanomaterials.

Keywords: splitting test, Brazilian test, indirect tensile strength, tensile strength, concrete strength, splitting concrete.

List of Symbols

BT   Brazilian test
ITT   Indirect tensile test
CS   Compression strength (f_c)
σ_G Griffith stress
D   Disk diameter
as   Aggregate size
α   Contact angle or angle subtended from the geometric center of the sample by the contact area
C   Curved portion of the lateral surface of a right circular cylinder
U   Uniform load distribution in the contact area
F   Flattened portion of the lateral surface of a right circular cylinder
P   Load project parallel to one another within the specimen

R   Load project radially to the axis that passes through the geometric center of the sample
CUR   Loading geometry with a contact characterized by C, U, and R
CUP   Loading geometry with a contact characterized by C, U, and P
FUP   Loadinggeometry with a contact characterized by F, U, and P
C_f^{CUR} Correction factor when using CUR loading geometry
C_f^{CUP} Correction factor when using CUP loading geometry
C_f^{FUP} Correction factor when using FUP loading geometry
TS   Tensile strength (σ_{TS})
ITS   Indirect tensile strength (σ_{ITS})
GF   Griffith function (f_G)
P_{max} Maximum applied load
t   Disk thickness

[1]Universidad Técnica Particular de Loja, UTPL, Loja, Ecuador.
*Corresponding Author; E-mail: vjgarcia2@utpl.edu.ec
[2]Universidad Nacional de Chimborazo, Riobamba, Ecuador.
[3]Universidad de Los Andes, Mérida, Venezuela.

1. Introduction

Concrete is the most widely used construction material. It is a composite material that is complex over a wide range of

length scales, ranging from nanometers to meters (Vorel et al. 2012). In general, failure in concrete structures, highway pavement, and dams, among other construction projects, can be attributed to some form of tensile stress. The tensile strength (TS) is determined by the direct tensile test or the ITT. The BT is an experimental test that permits an indirect inference of the TS even though it measures the indirect tensile strength (ITS). The ITS is related to the compression strength (CS), water-cement ratio, and age of the concrete, among other factors (Zain et al. 2002).

The BT is useful when experimenting with brittle or quasi-brittle materials that have a much greater CS than their TS and is effective elastically deforming material and that are susceptible to brittle ruptures, such as concretes, ceramics, rocks, coal, polymers, cemented carbides, and pharmaceutical products, among others. Also, the BT has been used in assessing the strength and durability recycled aggregate concrete, fine-aggregate concrete containing rice husk ash, and the effect of relative levels of mineral admixture on strength of concrete (Le et al. 2014; Mala et al. 2013; McNeil and Kang 2013; Yehia et al. 2015).

The BT is also called the diametrical compression test, ITT, splitting test, and split-tension test, among other names. The BT is straightforward and economic and can be used on cylindrical specimens (fabricated in molds or extracted concrete cores) or on flat disk-shaped specimens as well as cubes or prisms (Rocco et al. 2001). Also, the test can be performed with the same machine that is used to perform direct compression tests, and samples identical in shape and geometry as those used in direct compression can be employed. The BT was first prescribed by Fernando LLB Carneiro in Brazil (Carneiro 1943) and by Tsunei Akazawa in Japan (Akazawa 1943) in 1943, where the TS was measured in cylindrical concrete samples. In the BT, a flat, circular, solid disk is compressed with load concentrated on a pair of antipodal points. In this way, a tensile stress is induced in the direction perpendicular to the applied load, and it is proportional to the magnitude of the applied load. When the disk is a homogeneous, isotropic, elastic material, the induced tensile stress is greatest in magnitude at the geometric center of the disk. The stress trajectory near the geometric center and the shape of a typical *biaxial* compression and tension strength envelope of concrete, put forward that tensile stress at failure under a compression and tension stress ratio of −3 is nearly the same as the tensile stress at failure under *uniaxial* tension (Newman 2003). Thus the ITS is almost the same as the *uniaxial* TS. In this way, when the induced stress exceeds the TS, fracture initiates at the geometric center of the disk. In agreement with the Griffith criterion (Griffith 1920), the exact center of the disk is the only point at which the conditions for failure under tension are satisfied because, in this site, the tensile stress equals the uniaxial strength of the tested material (Erarslan et al. 2012). In fact, the BT result is accepted if fracture initiates at the center of the disk, and in this case, the measured value is representative of the TS of the tested material (Markides and Kourkoulis 2013). In the BT, the specimen must fail along the vertical line between compression points; otherwise, the observed failure mode is considered invalid (Li and Wong 2013). The test typically ends with a sudden, violent failure of the specimen when it reaches the maximum load due to the propagation of an unstable crack (Carmona and Aguado 2012).

Since its invention, the BT has motivated a wide variety of studies. One can gain an idea of its impact if one considers that the use of concrete test specimens has been standardized into norms in various countries, such as UNE-EN 12390-6, ASTM C-496, and CPC6 (Carmona and Aguado 2012). In 1951, the BT was standardized in the Japanese industry as a test method for determining the TS of concrete (Kourkoulis et al. 2013).

However, the validity of BT results has been a source of concern since the test's invention. Among the most crucial aspects is the point at which failure begins, which is related to the distribution of loads over the contact area (Markides and Kourkoulis 2013). In the BT, a stress field is induced, which is greatly controlled by the material properties of the specimen and the loading geometry (Erarslan et al. 2012). However, the BT is far from a universal test, and it is unknown whether a geometric configuration exists that favors effective, robust testing that is less sensitive to other experimental parameters other than the TS and CS of the specimen.

The objective of this work was finding out the most advisable loading geometry for an effective and robust characterization of the TS of concrete disks. The independent variables were the loading geometry, the angle subtended by the contact area, disk diameter and thickness, maximum aggregate size, and the sample CS. This study is important because, in traditional BT, cylindrical concrete samples are used, and its dimensions require the use of a relative "large" quantity of material. Even so, when we study composite concrete materials and nanomaterials, a standard protocol that optimizes the costs of proving samples does not exist, given that nanomaterials are still pricey even though they are used in low weight concentrations between 0.05 and 1%. At present, simple, low-cost, robust, and effective characterization techniques are required to make possible to study concrete that has been enabled to display new and improved properties with nanomaterials. Therefore, an effective and robust BT is of great importance for testing nanocomposite concrete (Birgisson et al. 2012; Hanus and Harris 2013; Mehdinezhad et al. 2013; Murty et al. 2013).

To achieve our goal, the theoretical and experimental aspects of the BT with three different loading geometries were reviewed. The equations that account for the stress–strain field developed within the disk were used to calculate (with the help of the GFC) the location where failure initiation is most likely depending on the angle subtended by the contact area and the loading geometry. Correction factors for the three loading setup were derived to adjust the measure ITS to be more representative of the uniaxial TS of the disk material. Three groups of experiments were performed to study the effect of the independent variables and their interactions. The experimental design for each

experiment corresponds with a two-levels and four factors of a factorial design. Each experiment involves only one loading setup. In the first groups of experiments, the CS was held constant, and the effects of contact angle, disk diameter, aggregate size, and thickness of the disk on the standard deviation of the measured ITS values were studied. In the second group of experiments, the disk diameter was held constant, and the influences of the following factors on the measured ITS values were studied: contact angle, CS, maximum aggregate size, and disk thickness. In the third groups of experiments, with only one loading geometry, the maximum aggregate size was held constant, and the effects of the following factors on the measured ITS values were studied: contact angle, CS, disk diameter and thickness of the disk.

2. Theoretical Aspects

2.1 Loading Geometry

BT results have shown evidence that crack begins near to the loading points, which occurs because stress–strain field singularity that develops near to the loading points, and the stresses developed exceeds those developed at the center of the disk (Huang, et al. 2014). In fact, one of the primary preoccupations when using the BT is the stress field that develops near the loading points. Therefore, for decades, researchers had performed experimental and theoretical studies to find out ways to reduce this stress concentration. In general, the studies have focused on improving the contact geometry between the loading block and the specimen (loading geometry) and on incorporating the elastic properties of the two bodies in contact. We defined the loading geometry bearing in mind: (1) the geometric shape of the contact area between the loading block and the specimens, (2) the load distribution on the contact area, and (3) the load projection toward the sample inside. If the bodies in contact can deform elastically and there are not cohesive forces between them, the contact is Hertzian. If the bodies in contact do not deform (or that their deformation is unimportant), the contact is rigid (Adams and Nosonovsky 2000; Kourkoulis et al. 2013; Markides and Kourkoulis 2012; Roux 1998).

The contact area between the loading block and the specimen can have the shape of the lateral geometric boundary of the sample (a curved (C) portion of the lateral surface of a right circular cylinder). Also, the contact area can be flat (a flattened (F) portion of the lateral surface of a right circular cylinder). The applied load could be such the pressure spread uniformly (U) over the contact area or non-uniformly (NU) following a parabolic distribution or a sinusoidal distribution. Also, the load could project forces parallel (P) to one another toward the inside of the specimen or project forces radially (R) to the axis that passes through the geometric center of the sample.

In a Hertzian contact, the load is at one point, and the pressure could be spread over the contact area in different ways, e.g., radially uniform, radially parabolic, and radially

sinusoidal (Adams and Nosonovsky 2000; Kourkoulis et al. 2013a, b; Markides and Kourkoulis 2012; Procopio et al. 2003; Roux 1998; Timoshenko and Goodier 1969).

When the contact is rigid, there is a linear dependence between the maximum applied load and the measured ITS. Whereas, if contact is Hertzian, a non-linear dependence develops between them (Awaji 1977; Kourkoulis et al. 2013a, b; Markides and Kourkoulis 2012). The use of mathematical analysis methods from elasticity theory had allowed the study of the stress field that develops within the sample under different loading geometry. Thus, there are available "simple" mathematical relations between the applied load and the ITS. Table 1 shows a summary of the loading geometries studied and the equations used to calculate the ITS. For the sake of comparison, Table 1 also shows the correction factors derived from our analysis. The derivations are in the following paragraphs. Note the correction factors derived in this work applied when the contact angle is greater than or equal to a value that serves as a threshold for defining the start of failure at the geometric center of the disk.

2.2 The Stress Field

The theoretical study of the stress field that develops in a flat circular disk subject to compression at two antipodal points at its geometric boundaries pertains to elasticity theory. Although the geometry of the disk and its boundary conditions are relatively straightforward, this has been a classic problem since 1883. In fact, an analysis of the stresses in a circular disk subject to compressive forces was first solved by Hertz in 1985 (Hertz 1895). In Hertz solution is evident that the stress distribution within the disk does not depend on the elastic constants of the solid. At present, it widely accepted that this is a characteristic that can be verified in any study on elasticity that implies a simply connected, two-dimensional region "studied as an isolated body" and composed of a homogeneous and isotropic solid (Sadd 2009). However, in the first half of the twentieth century, various mathematical methods were developed to determine the stress field in two-dimensional space (MacGregor 1933). These mathematical methods allowed the determination of the stress–strain field that develops within the solid, planar disk, where the geometric load configurations are more complex and diverse because the study of these cases is tough using classical elasticity theory. The basis of the new methods is the use of Airy functions (Love 1927), the strain function (Timoshenko 1924), the displacement function (Marguerre 1933), or the potential function (Carothers 1920; Nadái 1927).

Another lesson from Hertz´s solution is that the compression with loads concentrated at two antipodal points of a disk produces a high-stress concentration near the loading block. This stress concentration leads to failure initiation near to the loading block in certain materials (a situation that is undesirable when performing the BT). The load distribution over a small area at the geometric boundary of the disk could avoid the high-stress concentration near the loading block. Hondros (1959) calculated the whole stress

Table 1 Summary of the loading geometries studied and the equations used to calculate the Indirect tensile strength.

Loading geometry			Geometry	ITS	Correction factor	Correction factor calculated using Griffith function (GF)
S^a	D^b	P^c				
C	U	R		$\sigma_{TTS} = \frac{2P_{max}}{\pi Dt} C_f^{CUR}$	$C_f^{CUR} = \frac{\sin\alpha\cos^2\alpha}{\alpha}$ (Satoh 1986)	$C_f^{CUR} = \frac{\sin\alpha\cos^2\alpha}{\alpha}$; $\alpha \geq 20°$ (This paper)
C	U	P		$\sigma_{TTS} = \frac{2P_{max}}{\pi Dt} C_f^{CUP}$	$C_f^{CUP} = \left[1 - \left(\frac{b}{R}\right)^2\right]^{\frac{3}{2}} = \cos^3\alpha$; $\sin\alpha = \frac{b}{R}$ (Tang 1994)	$C_f^{CUP} = \frac{4\sin\alpha\left(\sin^2\alpha - 3\right)}{3\left(8\sin^3\alpha + 24\sin\alpha - 3\sin 2\alpha - 6\alpha\right)}$; $\alpha \geq 10°$ (This paper)
F	U	P		$\sigma_{TTS} = \frac{2P_{max}}{\pi Dt} C_f^{FUP}$	$C_f^{FUP} = \frac{\left(2A^2 + A + B\right)^2}{8(A+B)B}$; $A = \cos\alpha$; $B = \frac{\sin\alpha}{\alpha}$ (Wang et al. 2004)	$C_f^{FUP} = \frac{-\cos^2\alpha\sin\alpha}{(\sin\alpha\cos\alpha - 2\alpha)}$; $\alpha \geq 25°$ (Huang et al. 2014)
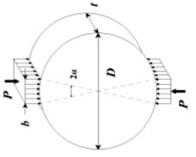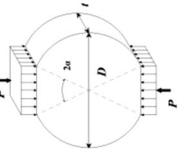
C and F account for a curved and flattened portion, respectively. U accounts for a uniform load distribution. R and P stand for radial and parallel projection, respectively. The *letter* D stand for disk diameter, t denotes the disk thickness, P is the maximum load at the moment of failure, α is the angle subtended by the contact area, and b is the horizontal distance over which the load is distributed in the CUP configuration. *GF* denotes the Griffith function.

[a] The shape of the contact area.
[b] Load distribution over the contact area.
[c] Load projection toward the interior of the sample.

field within a disk subjected to a load distributed radially and uniform over an arc (in a CUR loading geometry, see Table 1). Mathematically, the analyses of Hertz and Hondros are exact solutions for an elastic solid that satisfy the equilibrium equations. The analyses of Hertz and Hondros converge to the known relation of $\sigma_{ITS} = 2P_{max}/\pi D t$ when $x = 0$ and $y = 0$ and $2\alpha \to 0°$. Hondros in his solution assumed: (1) Small deformations. (2) No friction at the surface of contact. (3) The load applied at two antipodals points (for the Hertz equations), and (4) Load distributed over the arc of contact (for the Hondros equations) (Procopio et al. 2003). The robustness of the Hertz and Hondros solutions is evident when we consider that various researchers have arrived at the same conclusions using different mathematical methods (Frocht 1947; Timoshenko and Goodier 1951; Muskhelishvili 1954; Sokolnikoff 1956). More recently, it has been found the stress field developed within a specimen compressed through a CUP loading geometry (Wang et al. 2004) and a FUP loading setup (Huang et al. 2014), sees Table 2.

For the sake of clarity, Table 2 presents a summary of the stresses field developed in each of the load geometries shown in Table 1. Also, Table 1 shows the corresponding GF used calculating the location or region where conditions for failure initiation are satisfied. Because the ITT is "valid" only when a failure initiation occurs along the vertical line between compression points, the stress distribution along this line is of great interest. In polar coordinates, the component of the stress normal to the load line (σ_θ) and the component of stress along the load line (σ_r) are principal stresses (Hung and Ma 2003).

2.3 Failure Initiation

Throughout a BT, stresses concentrations occur in pores and cracks within the concrete disk. Stresses concentrations are ignored when the stress field is determined at the time of failure because the basic premise is the material is considered homogeneous, isotropic, and to exhibit linear elastic behavior before failure occurs (Li and Wong 2013; Mellor and Hawkes 1971).

If the material under analysis is brittle or quasi-brittle, then the location of failure initiation could be analyzed using the GFC (Griffith 1920). In agreement with the GFC, the geometric center of the disk is the only point at which the conditions are satisfied for tensile failure at a value equal to the uniaxial tensile strength (Huang et al. 2014).

Table 2 Main stresses and Griffith function for the three loading geometries shown in Table 1.

Loading geometry	Stress field	Griffith function, GF	Commentary
CUR	$\sigma_1 = \sigma_\theta = \frac{2P}{\pi D t}\frac{1}{\alpha}[A - B]$ $\sigma_3 = \sigma_r = -\frac{2P}{\pi D t}\frac{1}{\alpha}[A + B]$ $\tau_{r\theta} = 0; m = r/R$ $A = \frac{(1-m^2)\sin 2\alpha}{1-2m^2\cos 2\alpha + m^4}; B = \arctan\left(\frac{1+m^2}{1-m^2}\tan\alpha\right)$	$f_G(r;\alpha) = \frac{1}{4\sin\alpha}\left(\frac{A^2}{B}\right)$	Hondros (1959), Mellor and Hawkes (1971), Satoh (1986) and Hung and Ma (2003)
CUP	$\sigma_1 = \sigma_\theta = \frac{P}{\pi R t}\left[\frac{1}{2}A - C\right]$ $\sigma_3 = \sigma_r = \frac{P}{\pi R t}\left[\frac{1}{2}A - B\right]$ $\tau_{r\theta} = 0; m = r/R$ $A = \frac{1}{2}\frac{(2\alpha + \sin 2\alpha)}{\sin\alpha}; B = \frac{4}{1-m^2}; C = \frac{4(1+3m^2)\sin^2\alpha}{3(1-m^2)^3}$	$f_G(r;\alpha) = \frac{(B-C)^2}{8(A-B-C)}$	Satoh (1986), Wang et al. (2004), and Yoshiaki (1980)
FUP	$\sigma_1 = -\sigma_y\big|_{x=0} = \frac{P}{\pi R t \sin\alpha}$ $\left(\frac{B_1}{A_1} - C_1 + \frac{B_3}{A_3} - C_3\right) - \frac{P\cos\alpha}{\pi R t}$ $\sigma_3 = -\sigma_x\big|_{x=0} =$ $\frac{-P}{\pi R t \sin\alpha}\left(\frac{B_1}{A_1} + C_1 + \frac{B_3}{A_3} + C_3\right) - \frac{P\cos\alpha}{\pi R t}$ $\tau_{xy} = \frac{P}{2\pi R t \sin\alpha}\left(A^2\left(\frac{1}{A_1} - \frac{1}{A_2}\right) - B^2\left(\frac{1}{A_3} + \frac{1}{A_4}\right)\right)$ $A = R\cos\alpha + y; B = R\cos\alpha - y$ $C = x + R\sin\alpha; D = x - R\sin\alpha$ $A_1 = A^2 + D^2; B_1 = -AD; C_1 = \arctan(D/A)$ $A_2 = A^2 + C^2; B_2 = AC; C_2 = \arctan(C/A)$ $A_3 = B^2 + D^2; B_3 = -BD; C_3 = \arctan(D/B)$ $A_4 = B^2 + C^2; B_4 = BC; C_4 = \arctan(C/B)$	$f_G(y;\alpha) = \frac{-\left(\frac{B_1}{A_1} + \frac{B_3}{A_3}\right)^2}{4\sin\alpha(C_1 + C_3 + \sin\alpha\cos\alpha)}$	Huang et al. (2014)

Concrete typically contains aggregates and randomly and non-randomly oriented cracks in the form of micro-cracks. Crack initiate and propagate when the stress is above a certain threshold (Cai 2013).

If the compressive stress is "positive" and the value of the three principal stresses satisfies the relationship, $\sigma_1 \geq \sigma_2 \geq \sigma_3$, then the TS is represented by σ_{TS}. Failure initiates when the equivalent Griffith stress is greater than or equal to the uniaxial TS. In Eq. (1), we represent the equivalent Griffith stress (σ_G) and define the auxiliary function (g_G).

$$\sigma_G = \frac{(\sigma_1 - \sigma_3)^2}{8(\sigma_1 + \sigma_3)}; \quad g_G = (\sigma_1 + 3\sigma_3) \tag{1}$$

If $g_G \geq 0$, the GFC is expressed by Eq. (2).

$$\sigma_G \geq -\sigma_{TS} \tag{2}$$

If $g_G < 0$, the GFC is expressed by Eq. (3).

$$\sigma_G = |\sigma_3| \geq |\sigma_{TS}| \tag{3}$$

If $\sigma_G = -f_G \sigma_{TS}^* = -\sigma_{TS}$, where f_G is the GF and is defined for each load geometry in Table 2, $\sigma_{TS}^* = 2P_{max}/\pi Dt$ is also satisfied. At the center of the disk, the relationship between the principal stresses is $\sigma_1/\sigma_3 = -3$; thus, $g_G = 0$, and Eq. (2) leads to $\sigma_G = -\sigma_{TS}$, which represents the principle used to determine the TS from a BT (Wang et al. 2004). For this reason, the start of failure at the center of the disk is essential for the validity of a BT, i.e., is necessary if the test result is to correspond with the TS.

If failure initiates at the geometric center of the disk, then

$$\sigma_G = -\sigma_{TS} \tag{4}$$

$$\sigma_{TS} = -f_G(0;\alpha) \times \sigma_{TS}^* = -f_G(0;\alpha) \times \left(\frac{2P_{max}}{\pi Dt}\right)$$
$$= -C_f \times \frac{2P_{max}}{\pi Dt} \tag{5}$$

In this way, the correction factor when failure initiates at the geometric center of the disk is

$$C_f = f_G(0;\alpha)$$

To determine the region where failure initiates, we can calculate where occurs the maximum Griffith stress σ_G or, equivalently, for which value of m the function $f_G(m;\alpha_i)$ has its maximum value, where α_i is the contact angle and $m = r/R$. Thus,

$$\alpha = \{\alpha_0, \alpha_1, .., \alpha_i, ..\alpha_n\}$$
$$\downarrow$$
$$\frac{df_G(m;\alpha_i)}{dm} = 0 \quad \rightarrow m = m_i \tag{6}$$
$$\downarrow$$
$$[m_i;\alpha_i]$$

The m-α plot displays the normalized vertical distance between the point of failure initiation to the geometric center of the sample versus the angle subtended by the contact area. A normalized vertical distance close to one point up a location that is near to the contact area, and a value close to zero indicates a location that is near to the geometric center of the disk.

In Table 1 and Fig. 1, show the correction factor and the m-α plots for each of the CUR, CUP, and FUP loading geometries. Note in Table 1 that the procedure represented by Eq. (6) leads to the correction factor derived by Satoh (1986). In Fig. 1a, it can be seen that for small values of the contact angle, there is a natural tendency for failure to initiate in the vicinity of the loading block ($m = r/R \rightarrow 1$); we have already noted that elasticity theory predicts high-stress concentrations in regions near the loading block. Also, it can point out that as the contact angle increases, failure could initiate in locations closer to the geometric center of the disk ($m = r/R \rightarrow 0$). Thus, for example, for the CUP configuration, when the contact angle is greater than or equal to $10°$, the location of failure initiation suddenly moves to the geometric center of the disk (see Fig. 1a).

Figure 1b–d show how the magnitude of the correction factor C_f changes as a function of the contact angle α and in correspondence with the loading geometric (see Table 2). The α_{CUR}, α_{CUP}, and α_{FUP} are threshold values for the contact angle. Contact angle above the threshold values leads to failure initiation near to the geometric center of the disk. For the sake of clarity, the derived correction factors C_f^{CUR} and C_f^{CUP} together with the corrections factors reported in the literature are listed in Table 2. Note in Fig. 1b that the factor derived in this work for the CUR configuration coincides with the reported by Satoh (1986), whereas with the CUP setup, the factor derived in this paper differs from that reported by Tang (1994) when the contact angle is greater than approximately $15°$. In agreement with the method followed for their derivation, the correction factors can only be used when the contact angle has a value superior to the threshold contact angle (see Fig. 1a).

3. Experimental Aspects

Although there is no consensus among different technical norms and recommendations on the experimental conditions to carry out a BT, there are various proposals in the literature that are useful for achieving the best results. Table 3 shows a summary of the recommended practical considerations for mitigating the effect of stress concentration on the contact area, specimen diameter and thickness, aggregate size, and load velocity.

One way to reduce stresses on the contact area is by allowing plastic deformations or ensuring an inelastic con-
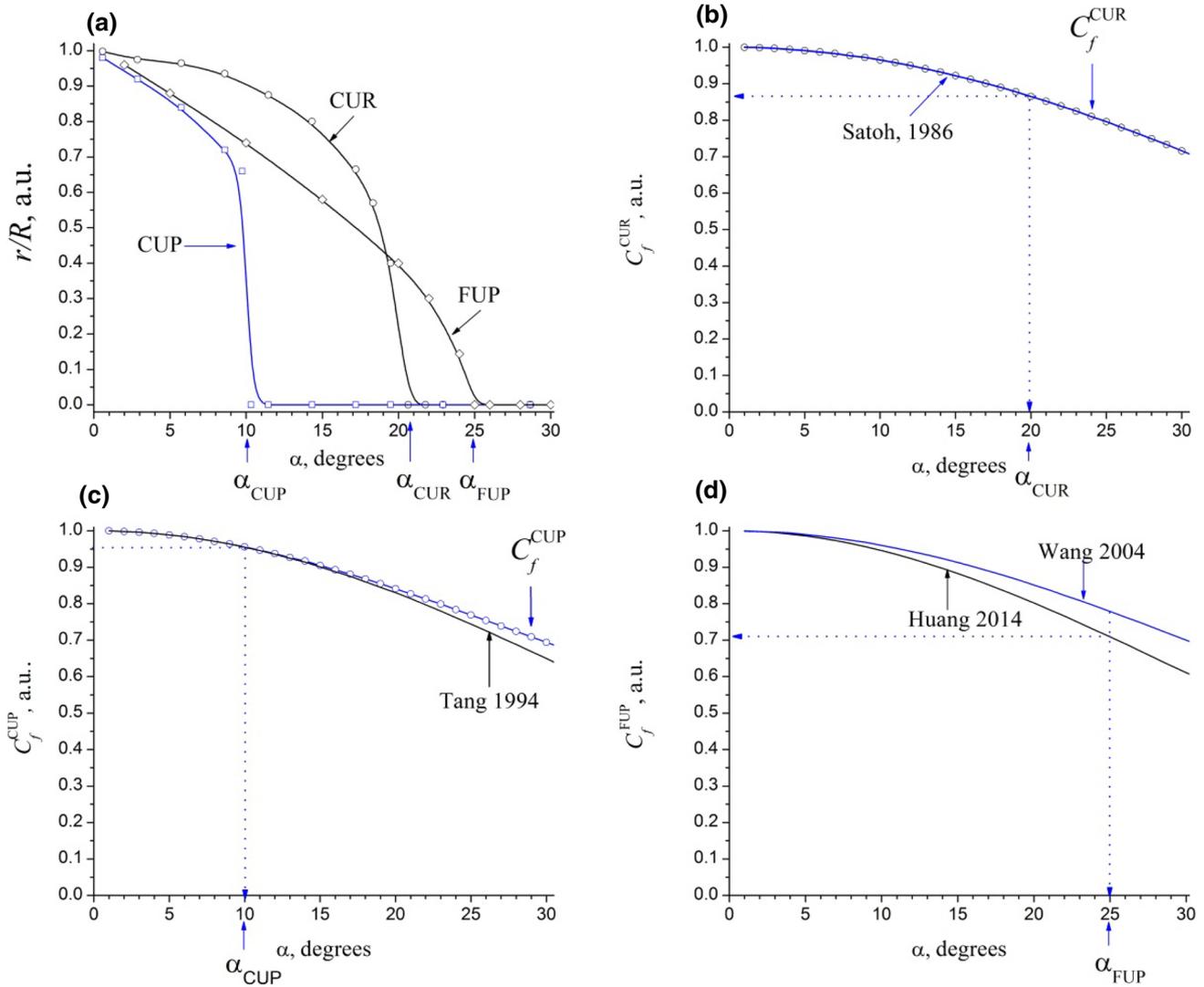
Fig. 1 a The plot illustrates how the angle subtended by the contact area determines the location with the greatest possibilities of failure initiation for each of the three load geometries studied. **b** Correction factor that must be used with the CUR setup; the factor derived by Satoh (1986) and the one derived in this work are shown. **c** Correction factor that must be used with the CUP loading geometry; the factor derived by Tang and the one derived in this work are shown. **d** Correction factor that must be used with the FUP setup; the factor derived by Wang et al. (2004) and the one derived by Huang et al. (2014) are shown.

tact; this is achieved by placing a cushion with a low yield point that distributes the load and reduces the stress concentration in this area. The cushion compensates for the irregularities of the geometric boundary of the disk. The objective is to distribute the load and to avoid local effects because of stress concentration at points of geometric irregularities in the disk. A cushion of comparatively soft material is placed between the specimen and the loading block of the machine to prevent excessive pressure. A more uniform load distribution is ensured when a thick cushion is used, and it deforms. When the cushion deforms, it creates a band of contact in the specimen that is nearly hydrostatic, which is extremely useful in calculations that assume a uniform load distribution. Placement of a cushion improves the stability of the test and avoids failures initiation near to the loading block caused by singularities in the stress field, although, the boundary conditions become ambiguous. While the ASTM norm

recommends the use of the cushion, the European norm EN 12390-6 requires a direct load on the cylinder (Wendner et al. 2014). The contact conditions are the main means that the experimenter has to influence the stress field to be developed within the specimen. Thus, for example, a cushion made of material, such as steel, can be selected for use on soft materials, and soft material, such as cardboard, can be chosen for use on more rigid samples. In practice, it is advisable to maintain a difference of five orders of magnitude between Young's moduli of the cushion and the sample. If an ideal contact is desired, the condition $E_s/E_c = v_s/v_c$ must be fulfilled, where v_s and E_s represent the Poisson ratio and Young's modulus of the sample, respectively, and v_c and E_c represent the Poisson ratio and Young's modulus of the cushion material, respectively (Andreev 1991). In practice, application of the load using the cushion simplifies the experiment without introducing undesirable effects (Andreev 1991).

Table 3 A summary of the recommended practical considerations for mitigating the effect of stress concentration on the contact area, specimen diameter, and thickness, aggregates size, and load velocity on the Brazilian Test results.

		Recommendation		Commentary
Cushion (c)	Length (thickness) (t_c)	$t_c \geq t$		Ideal contact $\rightarrow v_c E_s = v_s E_c$
	Thickness (g_c)	$g_c \approx 0.01 \times D$ $g_{min} = 0.254$ mm		v_s and E_s represent the Poisson ratio and Young's modulus of the sample, respectively
	Width (w_c)	$w_c \geq w$, length of contact arc, defined by 2α and by the loading set up		v_c and E_c represent the Poisson ratio and Young's modulus of the cushion material, respectively
	Materials	Cardboard Plywood Chipboard		Andreev (1991), ISRM (2007), ASTM (2008), Mellor and Hawkes (1971), Wong and Jong (2013), and Hawkes and Mellor (1970) $E_{YOUNG} = 10$ GPa; $v = 0.3$ Wang et al. (2014) and Zhu and Tang (2006)
Diameter (D)	$D = 100$ mm; $D = 150$ mm			ASTM (2003)
	$D_{min} = 3 \times as_{max}$			Japanese Industrial Standards (1951)
Maximum aggregates size (as)	$as \leq \frac{1}{3}D$			A size that does not interfere with the thickness dimension of the disk
				Japanese Industrial Standards (1951)
Thickness (t)	$0.2D \leq t \leq 0.7D$			ASTM (2008)
	$t \leq 0.2D \rightarrow$ plane stress $t \geq 0.5D \rightarrow$ plane strain			Aliha (2013) and Yu et al. (2006) Load concentrated in two antipodal points
	$t = 0.5D \rightarrow$ the volume under stress is similar to the volume under a typical uniaxial tensile test $t_{min} > 10$ mm			Mellor and Hawkes (1971)
Speed of displacement	0.2 inch/min $\rightarrow \leq 84.7$ μm/s			ASTM (2004, 2008),
	0.7 inch/min $\rightarrow \geq 169$ μm/s (viscoelastic samples)			
	The rate of loading is adjusted such that the duration of each test is between 2 and 3 min			Carmona (2009)

BS (1983), IS (1999), ISRM (2007), NBR (2010), NCh (1977), RILEM (1994), and UNE-EN (2001).

In the BT, one must consider the effect of the specimen thickness on the measured ITS value. It has been reported that measured ITS values increase when the disk thickness decreases. High values of tensile stress occur when the same ratio between load and thickness is maintained. In this way, the disk fails with lower than expected load values when the thickness increases (Komurlu and Kesimal 2014; Yu et al. 2006). A clear understanding of the effects of diameter, thickness, and their ratio can contribute to achieving better BT results (Guo et al. 1993). However, Wang et al. (2014) concluded that if the dominant failure mode occurs in the load plane, then the disk thickness has no substantial effect on the failure mode or the measured ITS when $t/D < 1$ (Wang et al. 2014). It is advisable to introduce low values of the t/D ratio such that the state of the stress in the specimen is one of the plane stresses in the loading plane. With a plane stresses the stress distribution across the thickness is more homogeneous (Lavrov et al. 2002). Yu et al. (2006)

adopted a 3-FEM and considered the effect of disk thickness ($0.2 \leq t/D \leq 1$) in the BT. Yu et al. (2006) concluded that the traditionally used formula becomes imprecise as the disk thickness increases. Thus, the authors proposed a correction factor (Y_c) to account for the effect caused by the three-dimensionality of the disk in a BT (Yu et al. 2006). Thus,

$$\sigma_{ITS} = \frac{2P_{max}}{\pi Dt} Y_c \text{ and } Y_c = 0.2621\left(\frac{t}{D}\right) + 1 \qquad (7)$$

Aliha (2013) also adopted 3D-FEM and determined a thickness correction factor for samples with a ratio of $t/D \leq 0.5$, see Eq. (8).

$$\sigma_{ITS} = \frac{2P_{max}}{\pi Dt} A_c \text{ and } A_c = 0.312\left(\frac{t}{D}\right) + 0.964 \qquad (8)$$

The loading geometry considered in the Aliha´s and Yu´s analysis included loads concentrated at antipodal points in a traditional setting. Therefore, Yu and Aliha 3D-FEM analysis ignored the effect of stress concentrations. Thus, the Yu and Aliha correction must be used with care when the loading setup is different from the traditional settings.

The most appropriate loading speed in a BT depends on the specimen behavior over time (Hashiba and Fukui 2015), if: (1) The strength increases with loading speed (i.e., depends on loading speed). (2) The strain increases when the stress is constant (creep). (3) The stress decreases when the strain remains constant (relaxation). To reduce the effect of loading speed, a BT is executed at low displacement speeds (≤ 84.7 μm/s), whereas in viscoelastic samples; a BT is carried out at greater speeds (≥ 169 μm/s) to reduce the effects of creep and relaxation. However, the BT has now expanded to high strain rate testing (using a split Hopkinson pressure bar) for measuring the dynamic tensile strength and dynamic fracture toughness of materials. Dynamic loads are characterized by high amplitude and short duration stress pulse or a high strain rate. Strain rates reported to be of relevance in cement-based materials range from 10^{-8} to 10^5 s^{-1} (Chen et al. 2014, 2016, 2017).

4. Experimental Design

Concrete mixes labeled as 21.1, 21.2, 30.1, and 30.2, contained an Ecuadorian pozzolanic Portland cement categorized as high initial strength type-HE according to ASTM C1157 (ASTM 2015) and as type-HE hydraulic cement according to the Ecuadorian technical norm NTE INEN 2380 (NTE-INEN 2011). Table 4 shows mix proportions and characteristic of the concrete specimens. The specimens characterization was carried out conforming standardized procedures using 150 mm × 300 mm cylindrical test pieces and lengths of 200 and 300 mm, respectively. The cylinder length was more than five times larger than the maximum size of the sums. The test parts were worked with concrete from the same blend, and the molds were filled with one layer. After 24 h, the test pieces were unfolded and stored in a tank of water kept at room temperature until the assessment date. The samples were tested seven days after being made. Before testing the specimens, the cylinders were thoroughly cut and sectioned into disks with thicknesses of 0.2 D and 0.5 D.

A 10-kN load cell was used to perform the BT, and the tests were carried out in the controlled displacement mode at a speed of 0.02 inches/min (84.7 μm/s). The loading speed was extremely low, and the test was conducted in quasi-static conditions (Tarifa et al. 2013). This displacement speed was selected after testing various speeds and

Table 4 Mix proportions and characteristics of concrete specimens.

Mix	21.1	21.2	30.1	30.2
	Content per m³ of concrete			
Cement (kg)	372	341	465	427
Water (L)	207	190	207	190
Sand (fine aggregate) (kg)	912	703	834	631
Gravel (coarse aggregate) (kg)	724	1052	724	1052
	Characteristics[a]			
Water-cement ratio	0.56	0.56	0.45	0.45
Maximum gravel size (inches)	3/8	3/4	3/8	3/4
CS (MPa)-theoretical value[b]	21	21	30	30
CS (MPa)-average strength values after 7 days[c]	34.7	33.98	45.6	44.52

[a] Aditek® 100 N additive was used in a proportion of 150 cc per 50 kg of cement to improve the workability of the blend when fabricating the cylinders.
[b] To perform the calculations, we followed the recommendation of the ACI of adding 8.5 MPa to each value.
[c] Each value is the average of three cylinders. CS account for compression strength.
Bold letters means the title of the columns and represent "mix label".

observing that this speed considerably reduced the zone of compression in the vicinity of the load block and that failure originated with greater frequency at the geometric center of the disk.

Table 5 shows the load geometries used in our experiments. The load blocks were fabricated using carbon steel. Blocks were designed such that the length of the contact area is subtended by the specified contact angle on a specific disk.

A factorial design with four-factor and each factor with two levels were carried out to study the effects of the loading geometry, contact angle, disk diameter and thickness, aggregate size, and CS have on the measured ITS values. The four factors have two possible values. Thus there are $2^4 = 16$ combinations or treatments. The possible factor values are coded as "−" and "."

Randomized trials were performed with all combinations that can be formed with the levels of factors to be investigated. Table 6 lists the factors and levels considered, and Table 7 shows all the tested combinations. To gain a better idea of the response variability (the variability of the measure ITS value), we randomly tested *five replicates* of each sample (with the same treatment). Thus, the total number of samples for each experiment was $16 \times 5 = 80$.

Table 8 shows the experimental design. The *first group of experiments*, 1.1, 1.2, and 1.3, was focused on the effects of the loading geometry, contact angle, and factors such as the diameter, thickness, aggregates size, and CS *on* the variability (standard deviation) of the measured ITS value. In this group, 240 concrete disk -2^4(treatments) ×5(replicas) ×3(load geometries)—were prepared and tested such that they exhibited the same theoretical CS (f_{c-}). Th *second*

Table 5 Loading geometries.

Geometry	α_1	α_2	
CUR	10°	22°	
CUP	5°	12°	
FUP	12°	25°	
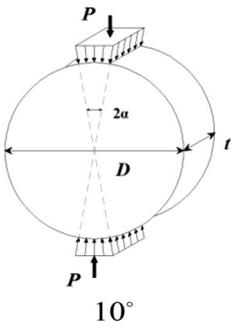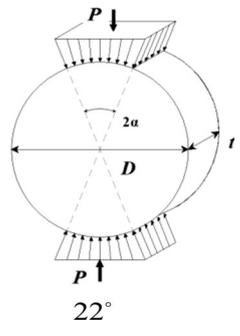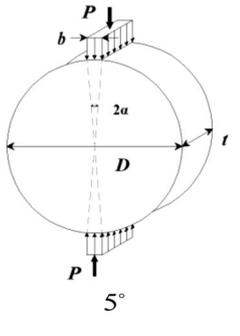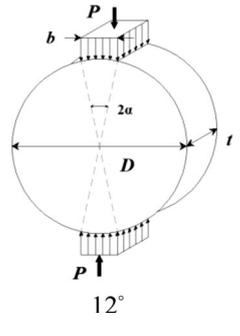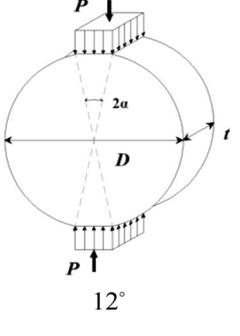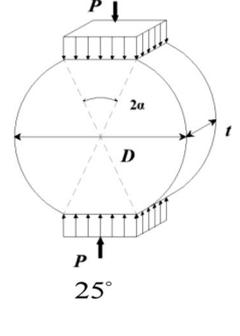
Table 6 Factors and levels.

Factor	Level		Units
	(−)	(+)	
CS (f_c)[a]	21	30	MPa
Diameter (D)	100	150	mm
Thickness (t)	0.2 D	0.5 D	mm
Maximum aggregates size (as)	9.5 (3/8)	19.1 (5/8)	mm (inches)
LG[b]–CUR; Contact angle (α)	10	22	degrees
LG[b]–CUP; Contact angle (α)	5	12	degrees
LG[b]–FUP; Contact angle (α)	12	25	degrees

[a] The theoretical value of the CS.

[b] Loading geometry.

Table 7 Factorial design of two levels and four factors[a].

Treatment	Factors			
	A	B	C	D
1	−	−	−	−
2	+	−	−	−
3	−	+	−	−
4	+	+	−	−
5	−	−	+	−
6	+	−	+	−
7	−	+	+	−
8	+	+	+	−
9	−	−	−	+
10	+	−	−	+
11	−	+	−	+
12	+	+	−	+
13	−	−	+	+
14	+	−	+	+
15	−	+	+	+
16	+	+	+	+

[a] Gutiérrez Pulido and Salazar (2008).

group of experiments, 2.1, 2.2, and 2.3, was concerned with the effects of the loading geometry, contact angle, and factors such as the diameter, thickness, aggregates size, and CS on the measured value of the ITS. In this group, 240 concrete disks −2⁴(treatments) × 5 (replicas) × 3 (load geometries)—were prepared and tested such that that have the same diameter ($D_−$). The *third experiment 3.1* was focused on the individual effects of contact angle on the CUP loading geometry and the effects of the CS, diameter, and thickness on the measured ITS values. In experiment 3.1, 80 concrete disks −2⁴(treatments) × 5 (replicas) ×1 (load geometric)— were prepared and tested with aggregates that had a size corresponding to the lowest value ($as_−$).

While testing the second group of experiments, 50% of the results achieved in the first group of experiments were taken into account, and 120 samples with a CS of f_{c+} were prepared and tested. A similar procedure was followed in experiment 3.1, in which 40 additional samples with diameter D were made and tested. All the data were processed using the statistical software Minitab® (MiniTab Inc. State College, PA, USA).

Before continuing, we will review several ideas that are essential to our experimental study. The *effect* of a factor is defined as the change observed in the ITS measured value (response variable) due to a change in the level of the said factor. The primary effect of a factor is the difference

Table 8 Experimental design.

Experiment	Geometry		CS[a]		Diameter		Thickness		Aggregates size	
	A				B		C		D	
	α_-	α	f_{c-}	f_c	D_-	D	t_-	t	as_-	as
LG[b]										
1.1 CUR	✓	✓	✓	–	✓	✓	✓	✓	✓	✓
1.2 CUP	✓	✓	✓	–	✓	✓	✓	✓	✓	✓
1.3 FUP	✓	✓	✓	–	✓	✓	✓	✓	✓	✓
	A		B				C		D	
2.1 CUR	✓	✓	✓	✓	✓	–	✓	✓	✓	✓
2.2 CUP	✓	✓	✓	✓	✓	–	✓	✓	✓	✓
2.3 FUP	✓	✓	✓	✓	✓	–	✓	✓	✓	✓
	A		B		C		D			
3.1 CUP	✓	✓	✓	✓	✓	✓	✓	✓	–	–

[a] Theoretical CS.
[b] Loading geometry (see Table 5).

between the average value of the measured ITS when the factor is at a low level and the average value of the measured ITS when the factor is at a high level. Moreover, it can be said that two factors interact significantly on the measured ITS value when the effect of one factor depends on the level of another factor. The *effect* of the interaction between two factors is denoted as *AxB*. The *effect* of the interaction is the difference between the average of the measured ITS value when both factors are at the same level, i.e., (−, −) or (,) and the average value of the measured ITS when the factors are at opposite levels, i.e., (−,) or (, −). Thus, the absolute values of the primary effects and, of the interactions are an important measure of the effect on the response variable (the measured ITS value). An analysis of variance (ANOVA) was performed to determine whether the effects were statistically significant (Gutiérrez Pulido and Salazar 2008).

The *ratio of the effect* offers a measure of the practical significance of the effect of a factor or of an interaction. It is used in variability analysis and is equal to the value obtained by dividing the standard deviation of the measured ITS values when the factor is at a high level by the standard deviation of the measured ITS values when the factor is at a low level. Thus, the value of the *ratio of the effect* indicates a proportional increase in the standard deviation of the measured ITS values when the factor changes from a low level to a high level. This quotient is used because the Minitab statistical software analyzes the natural logarithm of the standard deviation. The formula is *ratio of the effect* = exp(effect). For example, if the *effect* of factor A is 0.10, the *ratio of the effect* is exp(0.10), which is equal to 1.10517. This value is interpreted as an increase in the standard deviation by 1.10517 times (approx. 10.5%) when the factor changes from a low level to a high level (Minitab Inc. 2009).

The p value is used to help decide when to reject or accept the null hypothesis. The p value is equal to the probability of the null hypothesis. If we consider that the predefined significance is the maximum risk that we are prepared to take by rejecting the null hypothesis and that the observed or calculated significance corresponds to the p value, then the null hypothesis is rejected if the observed significance is less than the predefined significance. The acceptable level of risk is typically 0.050, and thus, the null hypothesis is usually rejected if the p value is less than or equal to 0.050. In other words, the p value indicates the possibility that the observed value occurs if the null hypothesis were true (Gutiérrez Pulido and Salazar 2008).

5. Experimental Results and Discussion

The *first group of experiments* deals with the effects of the contact angle, disk diameter and thickness, and the maximum aggregate size on the variability of the measured ITS value. The factors and interactions related to changes in the variability (standard deviation) of the measured ITS value

were finding out with the help of a least square regression model.

The *effect* of a factor was considered statistically significant if $p \leq 0.050$ and marginally significant if $0.050 < p \leq 0.100$. Table 9 shows the results of the first group of experiments. The results obtained in experiment 1.1 with the CUR loading geometry indicate that the contact angle, disk diameter, and "diameter-aggregates size-contact angle" interaction have a marginally significant contribution ($0.050 < p \leq 0.150$). The level of significance of the rest of the factors and interactions is greater than 0.150 ($p > 0.150$). The results show that the contact angle has the strongest *effect*, 0.715, and the *ratio of the effect* is that the standard deviation increases by a factor of 2 when the contact angle goes from the lowest level to the highest level. The "diameter-aggregates size-contact angle" interaction has the next strongest *effect*, 0.552. The diameter has a quantified *effect* of −0.398. The negative sign is interpreted as a decrease in the standard deviation when this factor goes from the low level to the high level. Therefore, the *ratio of the effect* is the standard deviation decreases by 0.672 when the diameter goes from the lowest level to the highest level. Thus, the results suggest that small contact angles and large values of the diameter are related to a lower standard deviation. However, lower contact angles do not induce failure initiation at the disk geometric center.

The results of experiment 1.2 with the CUP loading geometry show the contributions of the factors and their interactions are not statistically significant given that the

level of significance in all cases is greater than 0.150 ($p > 0.150$). This result suggests that the variabilities due to the different treatments are less than or equal to the variability due to error; in other words, there is no a significant effect due to the treatments. In particular, the results of Experiment 1.2 suggest that the high level of the contact angle is not related to the standard deviation of the result. However, we must bear in mind that a high contact angle would help initiate failure at the geometric center of the disk and that this condition is desirable for BT validity.

The results of experiment 1.3 with the FUP loading setup show that the contribution of disk thickness is significant ($p \leq 0.050$). Whereas, the disk diameter, aggregate size, "diameter-thickness" interaction, "aggregate size-thickness" interaction, "diameter-thickness-aggregates size" interaction, "diameter-thickness-contact angle" interaction, and "thickness-aggregates size-contact angle" interaction are marginally significant ($0.050 < p \leq 0.150$). Among them, the thickness has the strongest *effect*, −0.541. The *ratio of the effect* indicates that the standard deviation decreases by a factor of 0.582 when the thickness goes from the lowest level to the highest level (the two values attempted). The diameter has the next strongest effect, −0.416, whereby the standard deviation decreases by a factor of 0.660 when the diameter goes from the lowest level to the highest level. The minimum *effect* of all the factors is that of the aggregate size, −0.281. The results also showed that the contact angle has no significant contribution on the standard deviation of the measurement.

Table 9 Factors and interactions that affect the variability of measured Indirect tensile strength values in the group one of experiments[a].

	CUR			CUP			FUP		
	Effect	Ratio of the effect	p	Effect	Ratio of the effect	p	Effect	Ratio of the effect	p
(D)	−0.398	0.672	**0.139**	−0.101	0.904	0.707	−0.416	0.660	**0.062**
(t)	−0.144	0.866	0.350	0.137	1.146	0.625	−0.541	0.582	**0.048**
(as)	−0.072	0.931	0.564	0.110	1.117	0.685	−0.281	0.755	**0.092**
(α)	0.715	2.043	**0.078**	−0.088	0.915	0.740	−0.025	0.976	0.655
($D \times t$)	−0.261	0.770	0.208	−0.069	0.934	0.794	−0.347	0.707	**0.074**
($D \times as$)	0.340	1.405	0.162	−0.309	0.735	0.372	−0.088	0.916	0.276
($D \times \alpha$)	−0.030	0.970	0.789	−0.333	0.717	0.350	0.273	1.314	**0.094**
($t \times as$)	0.062	1.064	0.612	0.274	1.316	0.408	−0.210	0.811	**0.122**
($t \times \alpha$)	0.059	1.061	0.623	−0.171	0.843	0.557	−0.021	0.980	0.700
($as \times \alpha$)	−0.223	0.800	0.240	0.037	1.038	0.885	0.118	1.125	0.212
($D \times t \times as$)	0.025	1.025	0.826	0.012	1.012	0.964	−0.202	0.817	**0.127**
($D \times t \times \alpha$)	0.320	1.377	0.171	−0.224	0.799	0.471	0.318	1.375	**0.081**
($D \times as \times \alpha$)	0.552	1.736	**0.096**	−0.008	0.992	0.973	−0.030	0.971	0.570
($t \times as \times \alpha$)	−0.237	0.789	0.227	−0.147	0.863	0.603	0.175	1.191	**0.146**

[a] In this group, the CS was kept constant at the lowest level.
Bold letters mean values that are commented in text.

However, the FUP loading setup appears to lead to a measured ITS value that is related to some other factors and interactions, which, in practice, makes it undesirable.

The results of the first group of experiments do not show statistical evidence of the factors considered, nor do their interactions contribute significantly or marginally to variability in the measured ITS values when the CUP loading geometry is used.

Table 10 shows *the results of the group two of experiments*. First, an analysis was done to identify the factors that affect the variability in the measured ITS values when keeping the diameter at the lowest level.

The results of experiment 2.1 with the CUR loading setup show that the contact angle has a marginally significant contribution ($0.050 < p \leq 0.150$). The rest of the factors and interactions have a level of significance greater than 0.150. The contact angle has the strongest *effect*, 0.641. The *ratio of the effect* indicates that the standard deviation increases by a factor of 1.9 when the contact angle goes from the lowest level to the highest level. These results suggest that when the loading geometry corresponds with the CUR setup, small contact angles must be ensured to achieve a small standard deviation. However, lower contact angles do not favor failure initiation at the geometric center of the disk. Also, it is notable in this experiment that the CS does not contribute significantly to the standard deviation in the measured ITS value.

The results of experiment 2.2 with the CUP configuration show that the level of significance in all cases is greater than 0.150 ($p > 0.150$). Therefore, the high-level value of the contact angle does not contribute significantly to the standard deviation of the measured ITS value, but contributes to failure initiation at the geometric center of the disk.

The results of experiment 2.3 with the FUP loading geometry show the contribution of the CS to the standard deviation is significant ($p \leq 0.050$), whereas the degree of significance of the rest of the factors is greater than 0.150 ($p > 0.150$). The CS has the strongest effect, 0.611. The *ratio of the effect* is an increase in the standard deviation by a factor of 1.843 when the CS goes from the lowest level to the highest level. Thus, in the group two of the experiments, the diameter was held constant at the lowest level, and the results suggest once more that the CUP configuration is the most robust loading setup given that none of the factors or their interactions contributes significantly or marginal to the variability of the measured ITS values.

Table 11 shows the results of the group two of experiments obtained when we attempted to find the reduced model (RM) using least squares (LS) to predict the measured ITS value. For the RM, we used the factors and interactions that have a significant level of statistical significance. However, when the interactions have a relevant degree of significance, it is also necessary to include the factors that comprise them, even though the level of

Table 10 Study of the factors and their interactions that affect the variability of the measured Indirect tensile strength values in the group two of experiments[a].

	CUR			CUP			FUP		
	Effect	Ratio of the effect	p	Effect	Ratio of the effect	p	Effect	Ratio of the effect	p
(f_c)	0.201	1.222	0.411	0.010	1.010	0.974	**0.611**	1.843	**0.093**
(t)	−0.102	0.903	0.624	0.342	1.407	0.387	−0.292	0.747	0.191
(as)	−0.301	0.740	0.298	0.475	1.608	0.295	−0.154	0.857	0.337
(α)	**0.641**	1.898	**0.148**	−0.165	0.848	0.615	−0.117	0.889	0.416
($f_c \times t$)	−0.221	0.802	0.383	0.137	1.146	0.668	−0.100	0.905	0.469
($f_c \times as$)	0.113	1.120	0.593	0.056	1.058	0.853	0.041	1.042	0.729
($f_c \times \alpha$)	−0.103	0.903	0.622	−0.410	0.664	0.335	0.179	1.195	0.297
($t \times as$)	−0.116	0.891	0.585	0.062	1.064	0.837	−0.006	0.994	0.955
($t \times \alpha$)	−0.219	0.803	0.386	−0.050	0.951	0.867	−0.335	0.715	0.166
($as \times \alpha$)	−0.534	0.586	0.176	0.100	1.105	0.747	0.137	1.146	0.369
($f_c \times t \times as$)	−0.155	0.857	0.495	−0.200	0.818	0.554	0.000	1.000	0.998
($f_c \times t \times \alpha$)	0.040	1.040	0.838	−0.103	0.902	0.739	0.006	1.006	0.961
($f_c \times as \times \alpha$)	0.219	1.245	0.374	0.047	1.048	0.869	0.012	1.012	0.913
($t \times as \times \alpha$)	−0.182	0.834	0.443	−0.129	0.879	0.683	0.117	1.124	0.417

[a] In this group, the sample diameter was held constant at the lowest level.

Bold letters mean values that are commented in text.

Table 11 A reduced model for each loading geometry in the group two of experiments[a].

	CUR			CUP			FUP		
	Effect	Coeff.	p	Effect	Coeff.	p	Effect	Coeff.	p
Constant		5.1509	0.000		3.8009	0.000		5.3474	0.000
(f_c)	0.381	0.1903	0.096	**0.442**	0.2212	0.000	**1.257**	0.6287	0.000
(t)	0.130	0.0651	0.564	**−0.428**	−0.2141	0.000	0.340	0.1699	0.206
(as)	−0.053	−0.0266	0.811	0.067	0.0335	0.498	**−1.007**	−0.5036	0.000
(α)	**1.877**	0.9387	0.000	**0.747**	0.3735	0.000	**−0.945**	−0.4723	0.001
$(f_c \times t)$	**−0.529**	−0.2643	0.023	**−0.423**	−0.2114	0.000			
$(f_c \times as)$							−0.482	−0.2408	0.072
$(t \times as)$				−0.087	−0.0435	0.402			
$(f_c \times t \times as)$	**0.562**	0.2808	0.015						
$(f_c \times t \times \alpha)$				−0.119	−0.0594	0.238			
$(t \times as \times \alpha)$				0.146	0.0728	0.145			
R^2		65.89%			73.60%			53.21%	

[a] In this group, the sample diameter was held constant at the lowest level.
Bold letters mean values that are commented in text.

significance of these factors may not be relevant. Thus, the coefficients shown in Table 11 can be used to construct an equation that represents the ratio between the response (the measure ITS value) and the coded factors (−1;1) or (−,):

$$ITS = a_0 + a_1 D + a_2 t + a_3 as + a_4 \alpha + a_5 f_c t + a_6 f_c as$$
$$+ a_7 t\alpha + a_8 f_c as + a_9 f_c tas + a_{10} f_c t\alpha + a_{11} tas\alpha \tag{9}$$

where a_i are the coefficients presented in Table 11.

The RM that was found in experiment 2.1 with the CUR loading setup has an $R^2 = 65.89\%$. Thus, 65.89% of the variation in the measured ITS values are explained by the model, whereas in experiment 2.2 with the CUP loading geometry, the RM has an $R^2 = 73.60\%$ and in experiment 2.3 with the FUP loading setup, the model has an $R^2 = 53.21\%$.

The RM that was constructed with data from Experiment 2.1 (CUR configuration) shows that the contact angle has the greatest effect, 1.877, on the measured ITS value, followed by the effect of the "compressive strengths-thickness" interaction, −0.529. The CS have a marginal significance with an effect of 0.381. The maximum aggregate size has the least effect, −0.053. The RM that was obtained with data from experiment 2.2 (CUP setup) shows that the contact angle has the greatest effect (0.747) on the measured ITS values, followed by the CS (0.442) and the thickness (−0.428). The small effect is from the aggregate size (0.067).

The RM obtained with data from experiment 2.3 (FUP setup) shows that CS has the greatest effect (1.257) on the measured ITS values, followed by the effect of aggregate size (−1.007) and contact angle (−0.945). Although in experiment 2.3, the effect of CS is the strongest, the

predictability of the RM is the lowest (53.21%). Additionally, the effect of CS in experiment 2.2 (CUP setup) follows the strongest effect (0.442), and the predictability of its RM is the highest (73.60%). The effect of CS in experiment 2.1 (CUR setup) is in fourth place after the effect of contact angle, compressive strengths-thickness interaction, and compressive strengths-thickness-aggregate size interaction, with a value of 0.381.

The results of experiment 3.1 (CUP setup) are shown in Table 12. These results were achieved when we attempted to find the RM using LS to predict the measured ITS values. In this experiment, the aggregate size was held constant (at the lowest level), and the following factors were used as variables: disk diameter and thickness, CS, contact angle, and all their interactions.

The RM that was found has an $R^2 = 82.62\%$ and thus, the model explains 82.62% of the variation in the measured ITS values. The RM shows that the CS has the strongest effect (0.8095) on the measured ITS values, followed by the effect of contact angle (0.6341). Note that the results of experiment 3.1 (CUP setup) suggest:

1. When the diameter goes from the lowest level to the highest level, the estimated ITS value decreases by 0.2125 units.
2. When the thickness goes from the lowest level to the highest level, the estimated ITS value decreases by 0.3409 units.
3. If the CS goes from the lowest level to the highest level, the measured ITS value increases by 0.8095 units.
4. When the contact angle goes from the lowest level to the highest level, the measured ITS value increases by 0.6341 units.
5. The effect of the "diameter-CS" interaction results in an increase of 0.3510 in the measured ITS value when

one of the two factors is at the lowest level; the other is at the high level, and the factor that is at the high level goes to the lower level. Furthermore, the effect of this interaction results in a decrease of −0.3510 in the measured ITS value when the two factors are at the high level, and one of the two elements goes to the lower level.

6. The effect of the "CS-thickness" interaction results in a decrease of 0.3330 in the estimated ITS value when one of the two factors is at the lowest level; the other is at the high level, and the factor that is at the high level goes to the lower level. Additionally, the effect results in an increase of 0.3330 in the estimated ITS value when the two factors are at the high level, and one of the two factors changes to the low level.

7. The effect of the "thickness-contact angle" interaction is a decrease of 0.1778 in the estimated ITS value when one of the two factors is at the lowest level; the other is at the high level, and the factor at the highest level goes to the lower level. Additionally, the effect results in an increase of 0.1778 in the estimated ITS value when the two factors are at the high level, and one of the two elements goes to the lower level.

8. The effect of "thickness-CS-contact angle" interaction is interpreted using the same logic, in which the effect can be an increase or decrease by 0.1841 units in the measured ITS value.

Table 13 presents a summary of the *relative effects* of the factors and their interactions on the measured ITS value. The RM obtained with data from Table 12 is shown in

Table 12 Reduced model obtained in experiment 3.1 with the CUP loading geometry.

	CUP		
	Effect	Coeff.	p
Constant		$a_0 = 3.69198$	0.0000
(D)	−0.2125	$a_1 = -0.1062$	0.0200
(t)	−0.3409	$a_2 = -0.1704$	0.0010
(f_c)	**0.8095**	$a_3 = -0.4047$	0.0000
(α)	**0.6341**	$a_4 = -0.3170$	0.0000
$(D \times f_c)$	0.3510	$a_5 = -0.1755$	0.0000
$(t \times f_c)$	−0.3330	$a_6 = -0.1665$	0.0010
$(t \times \alpha)$	−0.1778	$a_7 = -0.0889$	0.0550
$(t \times f_c \times \alpha)$	−0.1841	$a_8 = -0.0921$	0.0420
R^2		82.62%	

In this group, the maximum aggregates size in the mix was held constant at the lowest level.
Bold letters mean values that are commented in text.

Table 13 A partial summary of the relative effects of the factors and their interactions on the measured Indirect tensile strength (ITS) value with the CUP loading geometry.

Factor/interaction	Change from () to ()	Relative effect on the value of *ITS*
D	$(-) \rightarrow ()$	↓
t	$(-) \rightarrow ()$	↓
f_c	$(-) \rightarrow ()$	↑
α	$(-) \rightarrow ()$	↑
$D \times f_c$	$(-, +);(+,-) \rightarrow (-,-);(-,-)$	↓
	$(+,+);(+,+) \rightarrow (-, +);(+,-)$	↑
$t \times f_c$	$(-, +);(+,-) \rightarrow (-,-);(-,-)$	↓
	$(+,+);(+,+) \rightarrow (-, +);(+,-)$	↑
$\alpha \times f_c$	$(-, +);(+,-) \rightarrow (-,-);(-,-)$	↓
	$(+,+);(+,+) \rightarrow (-, +);(+,-)$	↑

Table 14 Estimation of the Indirect tensile strength (ITS) value using the Reduced model in Eq. (10) and data from Table 12.

D	t	α	f_c	c	m	$m \times f_c$	$ITS = c + m \times f_c$
1	−1	−1	−1	3.5626	0.3036	−0.3036	3.2590
−1	−1	1	−1	4.3744	0.4878	−0.4878	3.8866
−1	1	−1	−1	3.3996	0.1548	−0.1548	3.2448
−1	1	1	−1	3.8558	**−0.0294**	0.0294	3.8852
1	−1	−1	−1	3.3502	0.6546	−0.6546	2.6956
1	−1	1	−1	4.1620	**0.8388**	−0.8388	3.3232
1	1	−1	−1	3.1872	0.5058	−0.5058	2.6814
1	1	1	−1	3.6434	0.3216	−0.3216	3.3218
−1	−1	−1	1	3.5626	0.3036	0.3036	3.8662
−1	−1	1	1	4.3744	0.4878	0.4878	4.8622
−1	1	−1	1	3.3996	0.1548	0.1548	3.5544
−1	1	1	1	3.8558	**−0.0294**	−0.0294	3.8264
1	−1	−1	1	3.3502	0.6546	0.6546	4.0048
1	−1	1	1	4.1620	**0.8388**	0.8388	5.0008
1	1	−1	1	3.1872	0.5058	0.5058	3.6930
1	1	1	1	3.6434	0.3216	0.3216	3.9650

Bold letters are commented in text.

(a) $f_c = 30$ MPa, $\alpha = 12°$, $f_c = 21$ MPa

(b) $f_c = 30$ MPa, $\alpha = 5°$, $f_c = 21$ MPa
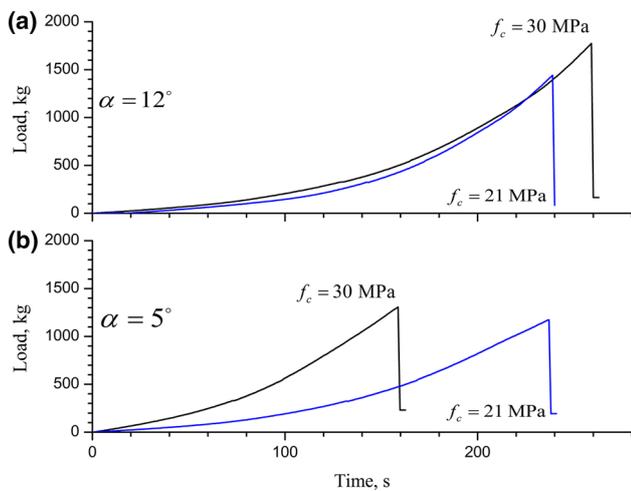
Fig. 2 The load vs time for CUP loading geometry when the specimen compression strength change from 21 to 30 MPa and the contact angle change from 12° (Fig. 2a) to 5° (Fig. 2b) and: $D = 100$ nm, $as = 3/8$ inch, $t = 20$ mm.

Eq. (10). The terms have been grouped according to the data in Table 14.

$$
\begin{aligned}
ITS &= c + mf_c \\
&= (a_0 + a_1 D + a_2 t + a_4 \alpha + a_7 t\alpha) \\
&\quad + (a_3 + a_5 D + a_6 t + a_8 t\alpha) f_c
\end{aligned}
\tag{10}
$$

The results in Table 14 suggest that if D is at its highest level (150 m), t is at its lowest level (30 mm), and α is at its highest level (12°), then these experimental conditions are related to a large response to changes of f_c. Thus, m in these experimental conditions assumes its highest value (0.8388), whereby a change in the response (the measured ITS value) would be more related to a change in the nature of the sample (in our case, to the value of f_c). Also, results in Table 14 suggest that the least favorable condition for a BT occurs when the diameter is the lowest (100 mm), the thickness is 50 mm, and the contact angle is 10°. In these conditions, a change from the low level to the high level of CS is related to a relatively small change in the response (ITS value).

Figure 2 sketches the load versus time for CUP loading geometry when the specimen compression strength change from 21 to 30 MPa and the contact angle change from 12° (Fig. 2a) to 5° (Fig. 2b).

6. Conclusions

The tendency to failure initiation near to the loading block is reduced by spreading the load uniformly over the contact area and by projecting the load parallel to one another within the disk. The focus of this study was the contact area between the loading block and the geometric boundary of the disk. Therefore, this study considered three frequently used BT loading geometries: CUR, CUP, and FUP setup.

For the failure initiation at the geometric center of the disk, it is necessary for the contact angle in the loading setup to be greater than or equal to the threshold value indicated in Fig. 1a (CUR: $\alpha \geq 20°$; CUP: $\alpha \geq 10°$; and FUP:

α ≥ 25°). However, the measured ITS values must be adjusted to get an idea of the uniaxial TS of the material, and the correction depends on the loading geometry. The GFC and the GF allowed to get mathematical expressions for the correction that apply on CUR, CUP, and FUP setup. More than 70 years have elapsed since the debut of the BT, and there are many practical recommendations reported in the literature. Nevertheless, the lack of further work regarding various loading geometries and the validity conditions of the test is evident. The results suggest that the CUP loading geometry with a contact angle of 12 or more degrees is the most advisable and robust setup for implementation of BT with concrete disks.

Acknowledgements

Funding

Compliance with Ethical Standards

Conflict of interest

The authors declare that they have no conflict of interest.

Open Access

References

Adams, G. G., & Nosonovsky, M. (2000). Contact modeling-forces. *Tribology International, 33,* 431–442. doi:10.1016/S0301-679X(00)00063-3.

Akazawa, T. (1943). New test method for evaluating internal stress due to compression of concrete (the splitting tension test) (part 1). *Journal of Japanese Civil Engineering Institute, 29,* 777–787.

Aliha, M. R. M. (2013). Indirect tensile test assessments for rock materials using 3-D disc-type specimens. *Arabian Journal of Geosciences.* doi:10.1007/s12517-013-1037-8.

Andreev, G. E. (1991). A review of the Brazilian test for rock tensile strength determination. Part II: Contact conditions. *Mining Science and Technology, 13,* 457–465. doi:10.1016/0167-9031(91)91035-G.

ASTM. (2003). C31/C 31M-03 Práctica Normalizada para Preparación y Curado de Especímenes de Ensayo de Concreto en la Obra. In *Book of standards Vol. 04.02 concrete and aggregates.* West Conshohocken, PA: ASTM International.

ASTM. (2004). C496 Standard test method for splitting tensile strength of cylindrical concrete specimens. In *Annual book of ASTM standards.* West Conshohocken PA: ASTM International.

ASTM. (2008). D3697-08 Standard test method for splitting tensile strength of intact rock core specimens. In *Annual book of ASTM standards.* West Conshohocken PA: ASTM International.

ASTM. (2015). C1157/C1157M-11 Standard performance specification for hydraulic cement. In *Book of standards Vol. 04.01 cement; lime; gypsum.* West Conshohocken, PA: ASTM International.

Awaji, H. (1977). Diametral compressive stress considering by the Hertzian contact. *Journal of Materials Science, Japan, 27*(295), 336–341.

Birgisson, B., Mukhopadhyay, A. K., Georgene, G., Khan, M., & Sobolev, K. (2012). *Nanotechnology in concrete materials: A synopsis.* Washington, DC. Retrieved from www.TRB.org.

BS. (1983). 1881-117 Testing concrete-Part 117. In *Method for determination of tensile splitting strength.* London: British Standards Institution.

Cai, M. (2013). Fracture initiation and propagation in a Brazilian disc with a plane interface: A numerical study. *Rock Mechanics and Rock Engineering, 46*(2), 289–302. doi:10.1007/s00603-012-0331-1.

Carmona, S. (2009). Efecto del tamaño de la probeta y condiciones de carga en el ensayo de tracción indirecta. *Materiales de Construcción, 59*(294), 7–18. doi:10.3989/mc.2009.43307.

Carmona, S., & Aguado, A. (2012). New model for the indirect determination of the tensile stress–strain curve of concrete by means of the Brazilian test. *Materials and Structures, 45,* 1473–1485. doi:10.1617/s11527-012-9851-0.

Carneiro, F. L. L. B. (1943). A new method to determine the tensile strength of concrete. In *5th meeting of the Brazilian Association for Technical Rules, 3d. Section,* (pp. 126–129). Associacao Brasileira de Normas Tecnicas—ABNT.

Carothers, S. D. (1920). The direct determination of stress. *Proceedings of the Royal Society of London, 97*(682), 110–123.

Chen, X., Ge, L., Zhou, J., & Wu, S. (2017). Dynamic Brazilian test of concrete using split Hopkinson pressure

bar. *Materials and Structures*. doi:10.1617/s11527-016-0885-6.

Chen, X., Shao, Y., Chen, C., & Xu, L. (2016). Statistical analysis of dynamic splitting tensile strength of concrete using different types of jaws. *Journal of Materials in Civil Engineering, 28*(11), 4016117.

Chen, X., Wu, S., & Zhou, J. (2014). Quantification of dynamic tensile behavior of cement-based materials. *Construction and Building Materials, 51,* 15–23. doi:10.1016/j.conbuildmat.2013.10.039.

Erarslan, N., Liang, Z. Z., & Williams, D. J. (2012). Experimental and numerical studies on determination of indirect tensile strength of rocks. *Rock Mechanics and Rock Engineering, 45,* 739–751. doi:10.1007/s00603-011-0205-y.

Frocht, M. M. (1947). *Photoelasticity*. New York: Wiley.

Griffith, A. A. (1920). The phenomena of rupture and flow in solids. *Philosophical Transactions of the Royal Society, A221,* 163.

Guo, H., Aziz, N. I., & Schmidt, L. C. (1993). Rock fracture-toughness determination by the Brazilian test. *Engineering Geology, 33,* 177–188. doi:10.1016/0013-7952(93)90056-I.

Gutiérrez Pulido, H., & Salazar, R. de la V. (2008). *Análisis y diseño de experimentos*. Igarss 2014 (2nd edn.). México, DF.: McGraw-Hill Interamericana. doi:10.1007/s13398-014-0173-7.2.

Hanus, M. J., & Harris, A. T. (2013). Progress in Materials Science Nanotechnology innovations for the construction industry. *Progress in Materials Science, 58*(7), 1056–1102. doi:10.1016/j.pmatsci.2013.04.001.

Hashiba, K., & Fukui, K. (2015). Index of loading-rate dependency of rock strength. *Rock Mechanics and Rock Engineering, 48*(2), 859–865. doi:10.1007/s00603-014-0597-6.

Hawkes, I., & Mellor, M. (1970). Uniaxial testing in rock mechanics laboratories. *Engineering Geology, 4,* 177–285.

Hertz, H. (1895). *Gesammelte Werke (Collected Works)*. Leipzig.

Hondros, G. (1959). The evaluation of poisson´s ratio and Young´s modulus of materilas of a low tensile resistance by the Brazilian test. *Australian Journal of Applied Science, 10*(3), 243–268.

Huang, Y. G., Wang, L. G., Lu, Y. L., Chen, J. R., & Zhang, J. H. (2014). Semi-analytical and numerical studies on the flattened Brazilian splitting test used for measuring the indirect tensile strength of rocks. *Rock Mechanics and Rock Engineering*. doi:10.1007/s00603-014-0676-8.

Hung, K. M., & Ma, C. C. (2003). Technical note: Theoretical analysis and digital photoelastic measurement of circular disks subjected to partially distributed compressions. *Experimental Mechanics, 43*(2), 216–224. doi:10.1177/0014485103043002011.

IS. (1999). 5816:1999 splitting tensile strength of concrete method (1st revision, reaffirmed 2008). In *CED 2: Cement and concrete*. New Delhi: Bureau of Indian Standards.

ISRM. (2007). Suggested methods for determining tensile strength of rock materials. In R. Ulusay & J. A. Hudson (Eds.), *The complete ISRM suggested methods for rock characterization, testing and monitoring: 1974–2006* (pp. 177–184). ISRM.

Japanese Industrial Standards. (1951). A-1113 Standard method of test for tensile strength of concrete.

Komurlu, E., & Kesimal, A. (2014). Evaluation of indirect tensile strength of rocks using different types of jaws. *Rock Mechanics and Rock Engineering*. doi:10.1007/s00603-014-0644-3.

Kourkoulis, S. K., Markides, C. F., & Chatzistergos, P. E. (2013a). The standardized Brazilian disc test as a contact problem. *International Journal of Rock Mechanics and Mining Sciences, 57,* 132–141. doi:10.1016/j.ijrmms.2012.07.016.

Kourkoulis, S. K., Markides, C. F., & Hemsley, J. A. (2013b). Frictional stresses at the disc–jaw interface during the standardized execution of the Brazilian disc test. *Acta Mechanica, 224*(2), 255–268. doi:10.1007/s00707-012-0756-3.

Lavrov, A., Vervoort, A., Wevers, M., & Napier, J. A. L. (2002). Experimental and numerical study of the Kaiser effect in cyclic Brazilian tests with disk rotation. *International Journal of Rock Mechanics and Mining Sciences, 39*(3), 287–302. doi:10.1016/S1365-1609(02)00038-2.

Le, H. T., Nguyen, S. T., & Ludwig, H.-M. (2014). A study on high performance fine-grained concrete containing rice husk ash. *Concrete Structures and Materials, 8*(4), 301–307. doi:10.1007/s40069-014-0078-z.

Li, D., & Wong, L. N. Y. (2013). The Brazilian disc test for rock mechanics applications: Review and new insights. *Rock Mechanics and Rock Engineering, 46*(2), 269–287. doi:10.1007/s00603-012-0257-7.

Love, A. E. H. (1927). *Mathematical theory of elasticity* (4th ed.). London: Cambridge University Press.

MacGregor, C. W. (1933). The potential function method for the solution of two-dimensional stress problems. *Transactions of the American Mathematical Society, 38*(1935), 177–186.

Mala, K., Mullick, A. K., Jain, K. K., & Singh, P. K. (2013). Effect of relative levels of mineral admixtures on strength of concrete with ternary cement blend. *International Journal of Concrete Structures and Materials, 7*(3), 239–249. doi:10.1007/s40069-013-0049-9.

Marguerre, K. (1933). Spannungsverteilung und Wellenausbreitung in der kontinuierlich gestutzten Platte. *Ingenieur-Archiv, 4,* 332–353.

Markides, C. F., & Kourkoulis, S. K. (2012). The stress field in a standardized Brazilian disc: The influence of the loading type acting on the actual contact length. *Rock Mechanics and Rock Engineering, 45,* 145–158. doi:10.1007/s00603-011-0201-2.

Markides, C. F., & Kourkoulis, S. K. (2013). Naturally accepted boundary conditions for the Brazilian disc test and the corresponding stress field. *Rock Mechanics and Rock Engineering, 46,* 959–980. doi:10.1007/s00603-012-0351-x.

McNeil, K., & Kang, T. H. K. (2013). Recycled concrete aggregates: A review. *International Journal of Concrete*

Structures and Materials, 7(1), 61–69. doi:10.1007/s40069-013-0032-5.

Mehdinezhad, M. R., Nikbakht, H., & Nowruzi, S. (2013). Application of nanotechnology in construction industry. Journal of Basic and Applied Scientific Research, 3(8), 509–519.

Mellor, M., & Hawkes, I. (1971). Measurement of tensile stregth by diametral compression of discs and snnuli. Engineering Geology, 5, 173–225. doi:10.1016/j.enggeo.2008.06.006.

Minitab Inc. (2009). Minitab statistical software. State College, PA, USA. Retrieved from www.minitab.com.

Murty, B. S. M., Shankar, P., Raj, B., Rath, B. B., & Murday, J. (2013). Nanoscience nanotechnology. In B. Raj (Ed.). New Delhi: Springer. doi:10.1007/978-3-642-28030-6 .

Muskhelishvili, N. I. (1954). Some basic problems of the mathematical theory of elasticity: fundamental equations plane theory of elasticity torsion and bending. Springer-science Business Media, B. V. doi:10.1007/s13398-014-0173-7.2.

Nadái, A. (1927). Darstellung ebener Spannungszustande mit Hilfe von winkeltreuen Abbildungen. Zeitschrift fur Physik, 41(1), 48–50.

NBR. (2010). 7222 Concreto e argamassa – Determinação da resistência à tração por compressão diametral de corpos de prova cilíndricos. Rio de Janeiro: ASSOCIAÇÃO BRASILEIRA DE NORMAS TÉCNICAS.

NCh. (1977). 1170: Of 77 Hormigón-Ensayo de tracción por hendimiento. Santiago de Chile: Instituto Nacional de Normalización.

Newman, J. B. (2003). Strength-testing machines for concrete. In J. B. Newman & B. S. Choo (Eds.), Advanced concrete technology set: Testing and quality. New York: Elsevier Butterworth Heinemann. doi:10.1016/b978-075065686-3/50265-2.

NTE-INEN. (2011). 2380:2011 Cemento hidráulico. Requisitos de desempeño para cementos hidráulicos. Quito Ecuador: Instituto Ecuatoriano de Normalización.

Procopio, A. T., Zavaliangos, A., & Cunningham, J. C. (2003). Analysis of the diametrical compression test and the applicability to plastically deforming materials. Journal of Materials Science, 38, 3629–3639. doi:10.1023/A:1025681432260.

RILEM. (1994). CPC6 Tension splitting of concrete specimen. In technical recommendation for the testing and use of construction materials (pp. 21–22). London: RILEM.

Rocco, C., Guinea, G. V., Planas, J., & Elices, M. (2001). Review of the splitting-test standards from a fracture mechanics point of view. Cement and Concrete Research, 31, 73–82. doi:10.1016/S0008-8846(00)00425-7.

Roux, S. (1998). Quasi-static contacts. In H. J. Herrmann, J.-P. Hovi, & S. Luding (Eds.), Physics of dry granular media (pp. 267–284). Dordrecht: Kluwer Academic Publishers.

Sadd, M. H. (2009). Elasticity theory, applications and numerics. New York: Elsevier Inc.

Satoh, Y. (1986). Position and load of failure by in Brazilian test: A numerical analysis by Griffith criterion. Journal of Materials Science, Japan, 140(36), 1219–1224.

Sokolnikoff, L. S. (1956). Mathematical theory of elasticity. New York: McGraw-Hill.

Tang, T. (1994). Effects of load-distributed width on split tension of unnotched and notched cylindrical specimens. Journal of Testing and Evaluation, 22(5), 401–409. doi:10.1520/JTE12656J.

Tarifa, M., Poveda, E., Yu, R. C., Zhang, X., & Ruiz, G. (2013). Effect of loading rate on high-strength concrete: Numerical simulations. In J. G. M. Van Mier, G. Ruiz, C. Andrade, R. C. Yu, & X. X. Zhabg (Eds.), FraMCoS-8 (pp. 953–963).

Timoshenko, S. (1924). The approximate solution of two dimensional problems in elasticity. Philosophical Magazine, 47, 1095–1104.

Timoshenko, S., & Goodier, J. N. (1951). Theory of elasticity. New York, PA: The Maple Press Company.

Timoshenko, S., & Goodier, J. N. (1969). Teoria de la elasticidad. Curso de fisica teorica. Elmsford: Pergamon Press.

UNE-EN. (2001). 12390-6 Ensayos de hormigón endurecido-Parte 6: Resistencia a tracción indirecta de probetas. Madrid España: Asociación Española de Normalización y Certificación.

Vorel, J., Šmilauer, V., & Bittnar, Z. (2012). Multiscale simulations of concrete mechanical tests. Journal of Computational and Applied Mathematics, 236, 4882–4892. doi:10.1016/j.cam.2012.01.009.

Wang, Q. Z., Jia, X. M., Kou, S. Q., Zhang, Z., & Lindqvist, P. A. (2004). The flattened Brazilian disc specimen used for testing elastic modulus, tensile strength and fracture toughness of brittle rocks: analytical and numerical results. International Journal of Rock Mechanics and Mining Sciences, 41, 245–253. doi:10.1016/S1365-1609(03)00093-5.

Wang, S. Y., Sloan, S. W., & Tang, C. A. (2014). Three-dimensional numerical investigations of the failure mechanism of a rock disc with a central or eccentric hole. Rock Mechanics and Rock Engineering, 47(6), 2117–2137. doi:10.1007/s00603-013-0512-6.

Wendner, R., Vorel, J., Smith, J., Hoover, C. G., Bažant, Z. P., & Cusatis, G. (2014). Characterization of concrete failure behavior: A comprehensive experimental database for the calibration and validation of concrete models. Materials and Structures. doi:10.1617/s11527-014-0426-0.

Wong, L. N. Y., & Jong, M. C. (2013). Water saturation effects on the Brazilian tensile strength of gypsum and assessment of cracking processes using high-speed video. Rock Mechanics and Rock Engineering. doi:10.1007/s00603-013-0436-1.

Yehia, S., Helal, K., Abusharkh, A., Zaher, A., & Istaitiyeh, H. (2015). Strength and durability evaluation of recycled aggregate concrete. International Journal of Concrete Structures and Materials, 9(2), 219–239. doi:10.1007/s40069-015-0100-0.

Yoshiaki, S. (1980). Master Degree Desertation. Tokio University.

Yu, Y., Yin, J., & Zhong, Z. (2006). Shape effects in the Brazilian tensile strength test and a 3D FEM correction. International Journal of Rock Mechanics and Mining Sciences, 43, 623–627. doi:10.1016/j.ijrmms.2005.09.005.

Zain, M. F. M., Mahmud, H. B., Ilham, A., & Faizal, M. (2002). Prediction of splitting tensile strength of high-performance concrete. *Cement and Concrete Research, 32,* 1251–1258. doi:10.1016/S0008-8846(02)00768-8.

Zhu, W. C., & Tang, C. A. (2006). Numerical simulation of Brazilian disk rock failure under static and dynamic loading. *International Journal of Rock Mechanics and Mining Sciences, 43,* 236–252. doi:10.1016/j.ijrmms.2005.06.008.